Journal of Materials Chemistry B

PAPER

View Article Online
View Journal | View Issue

Cite this: J. Mater. Chem. B, 2014, 2, 4346

Merging of covalent cross-linking and biomimetic mineralization into an LBL self-assembly process for the construction of robust organic–inorganic hybrid microcapsules

Chunyong Tian,[ab] Chunhong Zhang,[a] Hong Wu,*[ad] Yixuan Song,[a] Jiafu Shi,[c] Xiaoli Wang,[a] Xiaokai Song,[a] Chen Yang[a] and Zhongyi Jiang[abd]

Received 13th February 2014
Accepted 30th April 2014

DOI: 10.1039/c4tb00243a

www.rsc.org/MaterialsB

A mild and efficient method for the construction of robust organic–inorganic hybrid microcapsules was developed by merging of covalent cross-linking and biomimetic mineralization into a layer-by-layer (LBL) self-assembly process. The diatom cell-inspired microcapsule structure had a biocompatible inner organic layer which could create a suitable microenvironment for biologically active substances inside the microcapsules and an inorganic layer which could function as a supporting membrane to maintain the intact morphology of the microcapsules. When in 40% PSS solution, only 5% of the hybrid microcapsules were deformed indicating that the hybrid microcapsule had a higher mechanical stability. The combination of the advantages of both the organic layer and the inorganic layer was applied for the immobilization of catalase (CAT). After being reused 7 times, the CAT in the hybrid microcapsules retained 78% of its initial activity. A buffering effect was created by the capsule wall and the immobilized CAT had a higher pH stability than the free CAT. After storing for 45 days, the CAT in the hybrid microcapsules retained 78% of its initial activity. It is envisaged that the as-prepared hybrid microcapsules can be extended to many applications such as biocatalysis, drug/gene delivery and biosensor fields.

1. Introduction

Microcapsules with tailored structures and properties have attracted increasing attention owing to their multifunctions and potential applications in diverse fields.[1] Nanocatalysts, proteins, therapeutic compounds, *etc.* can be incorporated either in the microcapsule lumen or within the multilayer shells in a controlled fashion.[2] Since its introduction in 1991, the layer-by-layer (LbL) self-assembly technique has rapidly expanded to become a premier method for the preparation of nanoscale films with desired properties.[3] Microcapsule membranes can be formed by using the LbL self-assembly technique that relies on electrostatic interactions, hydrogen bonding, coordination bonding, charge transfer, molecular recognition, hydrophobic interactions, chemical reactions or a combination of these interactions.[4–14] Deposition of polyelectrolytes of opposite charges layer-wise on the surface of interest is currently the most extensively used method on account for several intrinsic advantages including the capability to exert molecularly precise, bottom-up control over film composition and thickness, and the capability to fabricate uniform, conformal coatings on the surfaces/interfaces of most topographically and topologically complex objects.[15] However, the charge-dependent interactions which stitch the film materials together can be compromised upon changes of the pH value or the ionic strength of the bulk solution, resulting in distortion of structure, impairment of function, or even degradation of films.

Increasing the number of the assembly layers can improve the stability of the polyelectrolyte microcapsules to some extent, but it is time-consuming and, what's more, the mass transfer resistance will be increased with the increasing layer numbers. Recently, covalent bonds have been formed to intensify the LBL self-assembly process. Post-treatments such as heating, UV irradiation and addition of specific chemical reagent(s) are usually necessary to form covalent bonds.[16,17] These processes are generally harmful to biologically active substances to be immobilized. Therefore, a mild and efficient method is appreciated especially in the biotechnology fields. Inspired by the

[a]Key Laboratory for Green Chemical Technology of Ministry of Education, School of Chemical Engineering and Technology, Tianjin University, Tianjin 300072, China. E-mail: wuhong@tju.edu.cn; Fax: +86 22 2350 0086; Tel: +86 22 2350 0086

[b]National Key Laboratory of Biochemical Engineering, Institute of Process Engineering, Chinese Academy of Sciences, Beijing 100190, China

[c]School of Environment Science and Engineering, Tianjin University, Tianjin 300072, China

[d]Collaborative Innovation Center of Chemical Science and Engineering (Tianjin), Tianjin 300072, China. Fax: +86 22 23500086

composition of adhesive proteins found in the holdfast pads of mussels, dopamine has been proved to be able to modify virtually any kinds of solid surfaces/interfaces.[18–23] Dopamine is such a biomolecule that contains catechol and amine functional groups and can polymerize at alkaline pHs to form a thin adhesive polydopamine film through the Michael-type addition and Schiff base reaction. The polydopamine film has a latent reactivity towards nucleophiles like amine and thiol groups. Furthermore, the adhesion ability and latent reactivity of the oxidized quinone form dopamine can be transplanted into a few polymers through covalent grafting methods.[24–26] The tethered catechol groups of the modified polymers can be used as reactive handles for the subsequent assembly of amine or thiol containing polymers, and organic capsules with enhanced mechanical stability can be constructed by this reactive assembly process.

Fabrication of the hybrid microcapsule wall is another approach to improve the stability of microcapsules. Hybrid microcapsule walls are usually prepared by the following three kinds of LbL assembly processes. The first approach is the liquid-phase alternative deposition of charged polyelectrolytes and oppositely charged inorganic nano-particles.[27,28] The second approach involves the coordination of polyvalent transition metal ions with soluble polymers having metal-binding sites.[11] The third approach inspired by the biomineralization process in nature involves the infiltration of polyelectrolyte multilayers with sol–gel precursors, confining the sol–gel reaction to the polyelectrolyte multilayers on the surface of templates.[29] The protoplast of a diatom cell is tightly enclosed by its silica-based cell wall which serves as an efficient defense against its predators physically. The subtle structure of the diatom cell provides an inspiration to build hybrid microcapsules with high mechanical stability. It has been found that the diatom silica is actually a composite material with long-chain polyamines as characteristic constituents.[30,31] The electrostatic interactions between the positively charged amines and the negatively charged species of $Si(OH)_4$ or SiO_2 in solution are the main driving forces for the deposition of the silica-based hybrid materials. To mimic the biosilicification process in the diatom cell, a range of synthetic polyamines, including poly(allylamine), poly(L-arginine), poly(L-lysine), poly(ethyleneimine), *etc.*, have been used to deposit silica-based materials through an *in situ* sol–gel process.[32–35] In our previous studies, we have tried to prepare LBL microcapsules *via* an alternative assembly of protamine and titania layers.[36] In addition, $(protamine/PSS)_n$/protamine/silica microcapsules have also been prepared for the encapsulation of catalase.[29]

In the present study, a novel, mild and efficient method for the construction of robust organic–inorganic hybrid microcapsules was developed by merging of covalent cross-linking and biomimetic mineralization into an LBL self-assembly process. More specifically, alginate was modified with dopamine through the covalent grafting method. Catechol containing dopamine-modified alginate (Alg-DA) and amine containing poly(ethyleneimine) (PEI) were used as reactive building blocks to prepare the inner organic layer (PEI/Alg-DA/PEI). PEI also functioned as an inducer for the mineralization of silicate on the surface of PEI/Alg-DA/PEI to construct the external inorganic layer (silica). Organic–inorganic hybrid microcapsules with high mechanical stability were obtained after template removal. Catalase (CAT) was immobilized in the hybrid microcapsules and the enzyme stability was investigated.

2. Experimental section

2.1. Materials

Catalase (hydrogen peroxide oxidoreductase; 2000–5000 units per mg protein EC.1.11.1.6) from bovine liver, poly(sodium 4-styrene sulfonate) (PSS, MW *ca.* 70 000), and poly(ethyleneimine) (PEI, MW *ca.* 750 000, 50 wt% aqueous solution) were purchased from Sigma-Aldrich Chemical Co. Dopamine hydrochloride was purchased from Yuancheng Technology Development Co. Ltd. (Wuhan, China). 1-Ethyl-3-[3-dimethylaminopropyl] carbodiimide hydrochloride (EDC) and *N*-hydroxysuccinimide (NHS) were purchased from Shanghai Medpep Co. Ltd. Calcium chloride ($CaCl_2$), sodium carbonate (Na_2CO_3), sodium alginate, sodium silicate (Na_2SiO_3), tris(hydroxymethyl)aminomethane (Tris), hydrochloric acid (HCl), sodium dihydrogen phosphate dihydrate ($NaH_2PO_4 \cdot 2H_2O$), sodium phosphate dibasic dodecahydrate ($Na_2HPO_4 \cdot 12H_2O$), sodium hydroxide (NaOH), ethylenediaminetetraacetic acid (EDTA), and hydrogen peroxide (H_2O_2, 30 wt%) were obtained from Guangfu Reagent Chemicals Co. Ltd. (Tianjin, China). All other reagents were of analytical grade and used without further purification. The water used in all experiments was treated by the Millipore Milli-Q purification system.

2.2. Synthesis of dopamine-modified alginate

Dopamine-modified alginate (Alg-DA) was prepared *via* EDC/NHS coupling chemistry as described in previous literature.[11] One gram of sodium alginate was dissolved in 100 mL of PBS buffer solution (50 mM, pH 5.5). To activate the carboxylic groups of alginate, 0.968 g of EDC and 0.581 g of NHS were added into the above solution under stirring at room temperature. Then, 1.915 g of dopamine was added into the above mixture and stirred gently for 12 h at room temperature under the protection of N_2. The product was precipitated with alcohol for three times followed by lyophilization to remove residual dopamine, EDC and NHS.

2.3. Preparation of organic–inorganic hybrid microcapsules

The organic–inorganic hybrid microcapsules were prepared by merging of covalent cross-linking and biomimetic mineralization into an LBL self-assembly process. PSS-doped $CaCO_3$ microparticles were prepared according to the co-precipitation method previously described in the literature[22] and used as sacrificial templates. Briefly, 16 mg PSS was completely dissolved in 8 mL Na_2CO_3 solution (0.33 M) in a beaker at room temperature. Then, an equal volume of $CaCl_2$ solution (0.33 M) was rapidly added under vigorous magnetic agitation, and stirred continuously for 30 s. After settling for 20 min, the deposit was centrifuged and washed three times with deionized

water. Finally, PSS-doped $CaCO_3$ microparticles with a spherical shape of about 5 μm in size were obtained.

The inner organic layer was formed by the reactive LBL self-assembly method using PEI and Alg-DA as the building blocks. A hundred milligram of PSS-doped $CaCO_3$ microspheres were alternately suspended in PEI solution (7 mL, pH 7.0, 0.5 wt%) for 10 min and Alg-DA solution (7 mL, 1.5 mg mL^{-1}) for another 10 min. Then the PSS-doped $CaCO_3$ microspheres were suspended in PEI solution again to capture amine groups on the surface of the microspheres. After each assembly process, the microspheres were washed three times with deionized water.

The external inorganic layer was formed through the biomimetic mineralization process. The PEI/Alg-DA/PEI covered PSS-doped $CaCO_3$ microspheres were homogeneously dispersed in silicate solution (7 mL, pH 7.5, 50 mM) and shaken continuously for 30 min. The organic–inorganic hybrid microcapsules were acquired after removing the $CaCO_3$ template with EDTA solution (pH 6.0, 50 mM). For comparison, $(PEI/Alg\text{-}DA)_2$ organic microcapsules were prepared according to the same procedure.

2.4. Immobilization of CAT in the lumen of the hybrid microcapsules

8 mg of CAT was dissolved in 2 mL Tris–HCl buffer solution (pH 7.0, 50 mM) and added into the $CaCl_2$ solution before the co-precipitation process. The CAT-encapsulated $(PEI/Alg\text{-}DA)_2$ and $(PEI/Alg\text{-}DA)_1$/PEI/silica microcapsules were prepared according to the same procedure as described above.

2.5. Characterization

HRSEM images of the microcapsules were recorded using a field emission scanning electron microscope (FESEM, Nanosem 430). Elemental analysis of the microcapsules was accomplished by an energy dispersive spectroscope (EDS) attached to the FESEM. TEM observation of the microspheres and microcapsules was performed on a JEM-100CX II instrument. Zeta-potentials of $CaCO_3$ microparticles after the deposition of different building blocks were measured by using a zetasizer Nano ZSP instrument. Solid-state ^{29}Si MAS NMR spectra of the $(PEI/Alg\text{-}DA)_1$/PEI/silica microcapsules were recorded by using a solid-state NMR spectrometer (NMR). Thermogravimetric analysis (TGA) of the $(PEI/Alg\text{-}DA)_1$/PEI/silica microcapsules was performed on a Perkin-Elmer Pyris analyzer. DSC200F3 was used to measure the glass transition temperatures of PEI/Alg and PEI/Alg-DA composites. The pore-size distribution of the $(PEI/Alg\text{-}DA)_1$/PEI/silica microcapsules was determined by nitrogen adsorption–desorption isotherm measurements performed at 77 K on a Tristar 3000 gas adsorption analyzer. Pore-size distribution curves were calculated on the basis of the adsorption branch of nitrogen isotherms using the Barrett–Joyner–Halenda (BJH) method. Confocal laser scanning microscopy (CLSM) images were taken with a Leica TCS SP5 microscope. The excitation wavelength was chosen as 488 nm according to the FITC-labeled enzyme.

2.6. Mechanical stability

The mechanical stability of $(PEI/Alg\text{-}DA)_2$ and $(PEI/Alg\text{-}DA)_1$/PEI/silica microcapsules was assessed by an osmotic pressure experiment. An equal amount of microcapsules was mixed in PSS aqueous solution of different concentrations. About 200 microcapsules were inspected at each PSS concentration. The percentage of deformed microcapsules was an indication of the mechanical stability of microcapsules. For comparison, $(PEI/Alg)_2$ microcapsules were prepared to investigate whether the covalent bonds between PEI and Alg-DA could improve the mechanical stability of the microcapsules.

2.7. Activity recovery of the enzyme immobilization process

The immobilization yield (eqn (1)) was used to describe the percentage of enzyme activity that was immobilized. The immobilized activity was determined by measuring the total residual enzyme activity that remained in the CAT solution after immobilization and by subtracting this activity from the total starting activity.

$$\text{Immobilization yield } (\%) = 100 \times \frac{\text{immobilized activity}}{\text{starting activity}} \quad (1)$$

The immobilization efficiency was the percentage of observed activity of the immobilized activity (eqn (2)).

$$\text{Immobilization efficiency}(\%) = 100 \times \frac{\text{observed activity}}{\text{immobilized activity}} \quad (2)$$

Activity recovery was the product of immobilization yield and immobilization efficiency and used to evaluate the immobilization process by comparing the activity of the immobilized CAT with the total starting activity of the free CAT (eqn (3)).

$$\text{Activity recovery } (\%) = 100 \times \frac{\text{observed activity}}{\text{starting activity}} \quad (3)$$

The activity of free and immobilized CAT was determined by measuring the decrease in the absorbance of hydrogen peroxide at 240 nm in 3 min due to the decomposition of H_2O_2.

2.8. Kinetic parameters (K_m and V_{max})

K_m and V_{max} for the free and immobilized CAT were determined using the Michaelis–Menten model given by eqn (4).

$$\frac{1}{V} = \frac{K_m}{V_{max}} \times \frac{1}{[S]} + \frac{1}{V_{max}} \quad (4)$$

where V (mM min^{-1}) is the initial reaction rate, [S] (mM) is the initial substrate concentration, V_{max} (mM min^{-1}) is the maximum reaction rate attained at an infinite initial substrate concentration and K_m (mM) is the Michaelis–Menten constant.

2.9. Stability of the immobilized enzyme

To investigate the recycling efficiency of the immobilized CAT, the immobilized CAT was collected after each reaction batch, washed with Tris–HCl (50 mM, pH 7.0) buffer to remove any

residual substrates and then added into the next reaction cycle. The reusability of immobilized CAT was explored by measuring the enzyme activity in each successive reaction cycle and expressed by recycling efficiency.

The effects of pH and temperature on the activity of free and immobilized CAT were determined by measuring the residual activity of CAT at 30 °C in Tris–HCl (50 mM, pH 7.0) after being exposed to different temperatures (30–70 °C) and pHs (4.0–9.0) in 50 mM Tris–HCl for 2 h.

Free and immobilized CAT were stored in Tris–HCl (50 mM, pH 7.0) at 4 °C for a certain period of time. The storage stability was compared in terms of storage efficiency defined as the ratio of the activity of free or immobilized CAT after storage to their initial activities.

3. Results and discussion

3.1. Fabrication and characterization of hybrid microcapsules

As illustrated in Fig. 1, a mild and efficient method of merging of covalent cross-linking and biomimetic mineralization into an LBL self-assembly process was developed to prepare robust organic–inorganic hybrid microcapsules. PSS-doped porous $CaCO_3$ microspheres were used as sacrificial templates. The doping of PSS helped to maintain the homogeneity of the morphology of $CaCO_3$ microspheres and rendered the surface of $CaCO_3$ microspheres with a negative charge. It has been demonstrated that calcite crystals are formed where the (001) surface is exposed. However, in PSS solution, the styrene sulfonate unit can bind to the (001) surface strongly, thus stabilizing the vaterite phase of $CaCO_3$, which is important to maintain the morphology of $CaCO_3$ microspheres.[37] The negative charge on the surface could not only prevent the aggregation of the microspheres driven by the decrease of the Gibbs free energy, but also enable the self-assembly of the positively charged PEI onto the surface of the templates.

For the fabrication of the inner cell membrane-like organic layer, the building blocks for self-assembly, PEI and Alg-DA, were firstly pre-assembled on the surface of the PSS-doped $CaCO_3$ templates through electrostatic attractions and then cross-linked through a nucleophilic attack between the amine groups on PEI and the C5 carbon atoms of catechol groups on Alg-DA, during which the Michael-type addition and Schiff base reaction could intensify the assembly process significantly (Fig. 1 (inner)).

The outmost sublayer of the organic layer was amine containing positively charged PEI, which could adsorb the silicon precursor with negative charges, silicate, *via* electrostatic and hydrogen bonding interactions. With the increase of the precursor concentration around the PEI layer, the hydrolysis and condensation process occurred to form Si–O–Si bonds. More and more silica accumulated around the PEI layer and then aggregated with other adjacent precursors, ultimately resulting in the formation of silica particles and eventually a compact cell wall-like inorganic silica layer.

The whole assembly process was monitored by measuring the surface zeta-potential of $CaCO_3$ microparticles before and after the deposition of the different building blocks. As shown

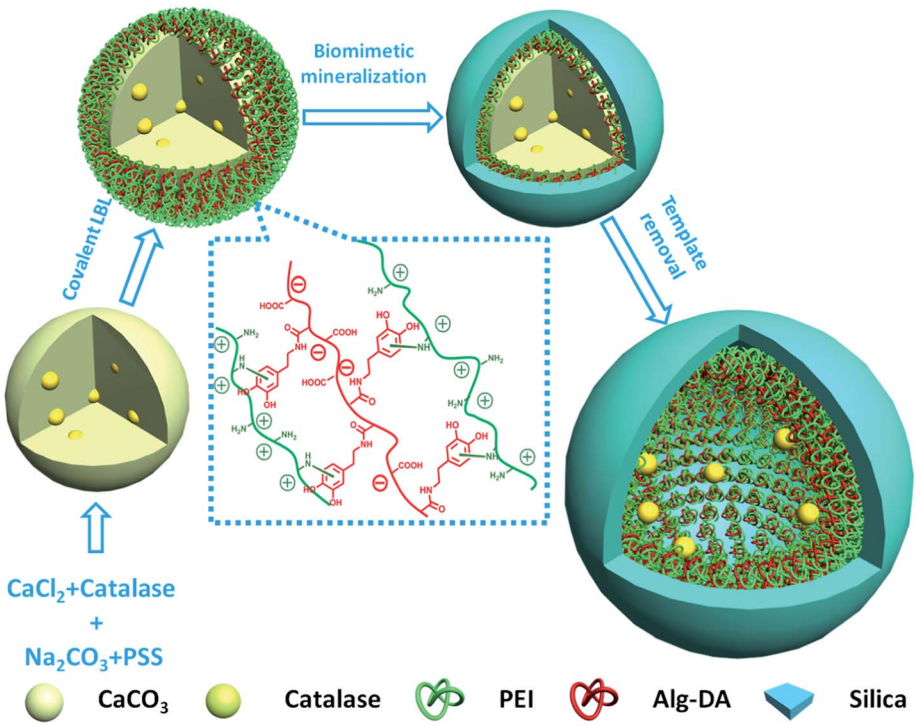

Fig. 1 Schematic representation of the fabrication procedure of the $(PEI/Alg\text{-}DA)_1PEI$/silica microcapsule and the fabrication principle of the inner organic layer of the hybrid microcapsule (inner).

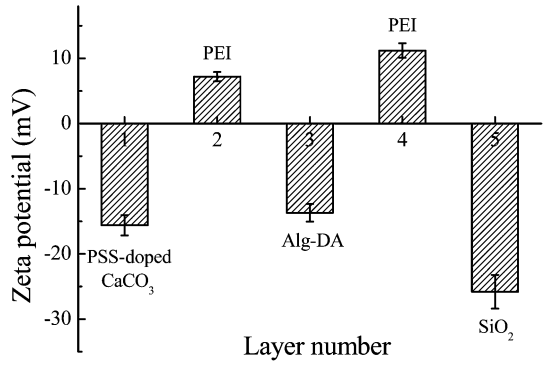

Fig. 2 Surface zeta-potentials of $CaCO_3$ microparticles after deposition of different building blocks.

in Fig. 2, the initial zeta-potential of $CaCO_3$ was about −15.6 mV. With the alternative deposition of PEI and Alg-DA, the zeta-potential changed between 10 mV and −15 mV. After mineralization, the surface zeta-potential decreased to −25.8 mV, indicating that silica was formed on the surface of the microparticles.

The organic–inorganic microcapsules were obtained after the $CaCO_3$ microspheres located at the core of the LbL assembly composites were dissolved by EDTA solution. The complex of Ca^{2+} with EDTA could easily permeate through the porous multilayers.

The SEM images of $(PEI/Alg\text{-}DA)_2$ and $(PEI/Alg\text{-}DA)_1/PEI/$ silica microcapsules (microparticles) are shown in Fig. 3. The $(PEI/Alg\text{-}DA)_2$ (Fig. 3(a)) and $(PEI/Alg\text{-}DA)_1/PEI/silica$ (Fig. 3(b) and (c)) microparticles were spherical. And the surface of the $(PEI/Alg\text{-}DA)_1/PEI/silica$ microparticle was covered with nanoparticles, while the surface of the $(PEI/Alg\text{-}DA)_2$ particle was smooth. The $(PEI/Alg\text{-}DA)_2$ microcapsules collapsed completely and some even broke after drying (Fig. 3(d) and (e)), suggesting the hollow structure and low mechanical strength of the organic microcapsules. The $(PEI/Alg\text{-}DA)_1/PEI/silica$ microcapsules did not collapse so severely as the pure organic microcapsules and no breaking occurred (Fig. 3(f) and (g)), suggesting that the hybrid microcapsules had a higher mechanical strength than the organic microcapsules. The surface of the organic microcapsules was smooth, indicating that the building blocks were deposited homogeneously. The surface of the hybrid microcapsules was rough. The external inorganic layer was composed of silica nanoparticles with a diameter of about 50 nm (Fig. 3(h)). The SEM image of the cross-section of the $(PEI/Alg\text{-}DA)_1PEI/silica$ microcapsule showed that the thickness of the microcapsule wall was *ca.* 200 nm (Fig. 3(i)). TEM images (Fig. 4) further confirmed the hollow and unbroken structure of the hybrid microcapsules.

Energy dispersive spectroscopy (EDS) analysis of $(PEI/Alg\text{-}DA)_2$ and $(PEI/Alg\text{-}DA)_1/PEI/silica$ is shown in Fig. 5. The appearance of the peak of N element confirmed the involvement of PEI in the assembly procedure. The appearance of the peaks of S element in both of the two kinds of microcapsules was attributed to the existence of PSS in the lumen of the microcapsules that did not permeate into the bulk water solution

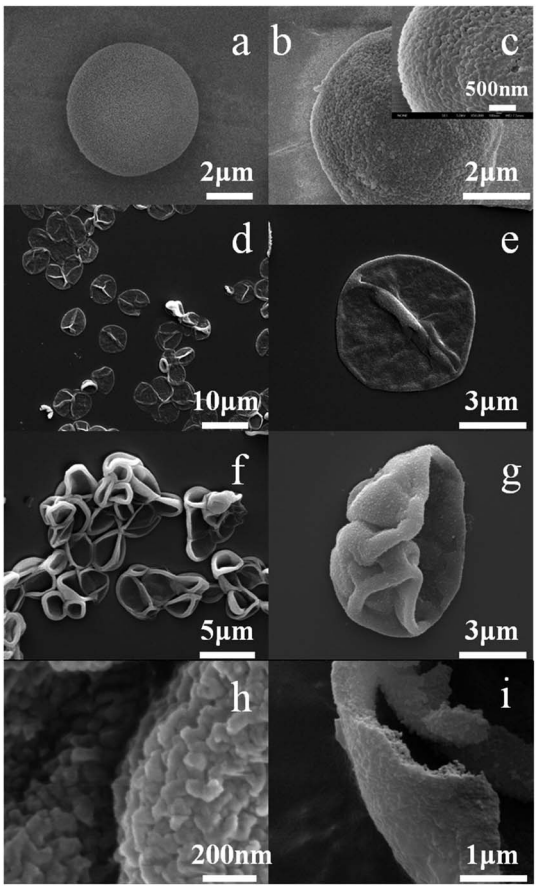

Fig. 3 SEM images of the $(PEI/Alg\text{-}DA)_2$ microparticle (a), $(PEI/Alg\text{-}DA)_1PEI/silica$ microparticle (b and c), $(PEI/Alg\text{-}DA)_2$ microcapsules (d), $(PEI/Alg\text{-}DA)_1PEI/silica$ microcapsules (f), enlarged SEM images of the single $(PEI/Alg\text{-}DA)_2$ microcapsule (e), single $(PEI/Alg\text{-}DA)_1PEI/silica$ microcapsule (g), SEM image of the surface morphology of the $(PEI/Alg\text{-}DA)_1PEI/silica$ microcapsule (h), and SEM image of the cross-section of the $(PEI/Alg\text{-}DA)_1PEI/silica$ microcapsule (i).

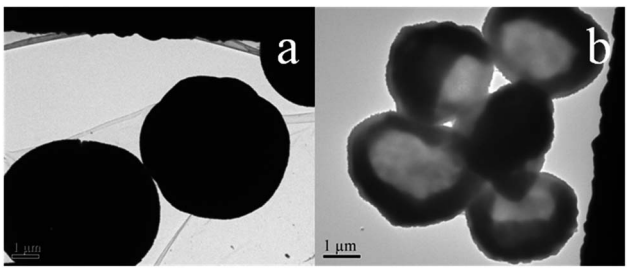

Fig. 4 TEM images of $(PEI/Alg\text{-}DA)_1PEI/silica$ microparticles (a) and $(PEI/Alg\text{-}DA)_1PEI/silica$ microcapsules (b).

during the washing procedure. The rejection of the capsule wall to PSS (large molecule) can be used to assess the mechanical stability of the capsules in the osmotic pressure experiment. The prevention of PSS from leaching also suggested the feasibility of enzyme (CAT, large molecule) entrapment in the lumen of the capsules. The appearance of the Si peak in the hybrid microcapsules confirmed that the silica layer was coated on the organic layer successfully.

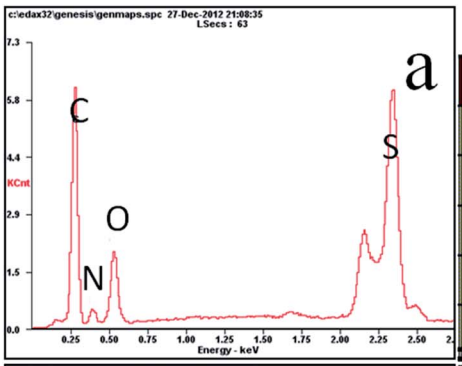

Element	Wt%	At%
CK	35.15	55.72
NK	04.35	05.91
OK	04.11	04.89
SK	56.39	33.48
Matrix	Correction	MThin

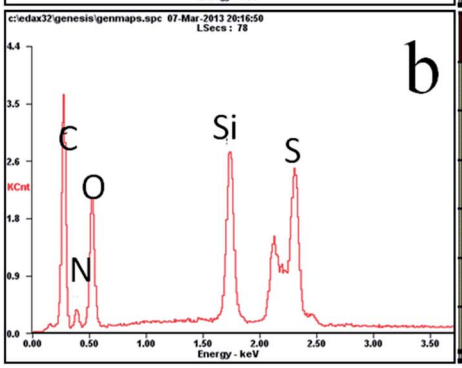

Element	Wt%	At%
CK	19.07	32.51
NK	02.75	04.03
OK	16.87	21.59
SiK	30.22	22.03
SK	31.08	19.85
Matrix	Correction	MThin

Fig. 5 EDS spectra of $(PEI/Alg\text{-}DA)_2$ (a) and $(PEI/Alg\text{-}DA)_1PEI$/silica (b) microcapsules.

The chemical structure of the as-formed silica at the atomic scale was studied by ^{29}Si NMR and is shown in Fig. 6 to analyze the degree of silicate condensation catalyzed by PEI. The four main peaks at −93, −98, −102.5 and −110.5 ppm were attributed to Q^1 [$Si(OSi)(OH)_3$], Q^2 [$Si(OSi)_2(OH)_2$], Q^3 [$Si(OSi)_3(OH)$], and Q^4 [$Si(OSi)_4$] with relative percentages of 13.8%, 6.7%, 53.4% and 26.1%, respectively. The high content of Q^3 and Q^4 adding up to 79.5% indicated a fairly high condensation degree of silanols, revealing that a well-condensed silica shell was generated.

The TGA curve of the hybrid microcapsules is shown in Fig. 7(a). The ~8.8% weight loss up to 300 °C (stage 1) was attributed to the physically adsorbed water and bound water

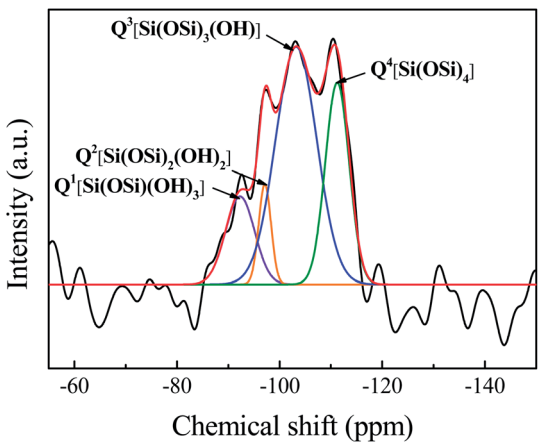

Fig. 6 ^{29}Si NMR of the $(PEI/Alg\text{-}DA)_1PEI$/silica microcapsules.

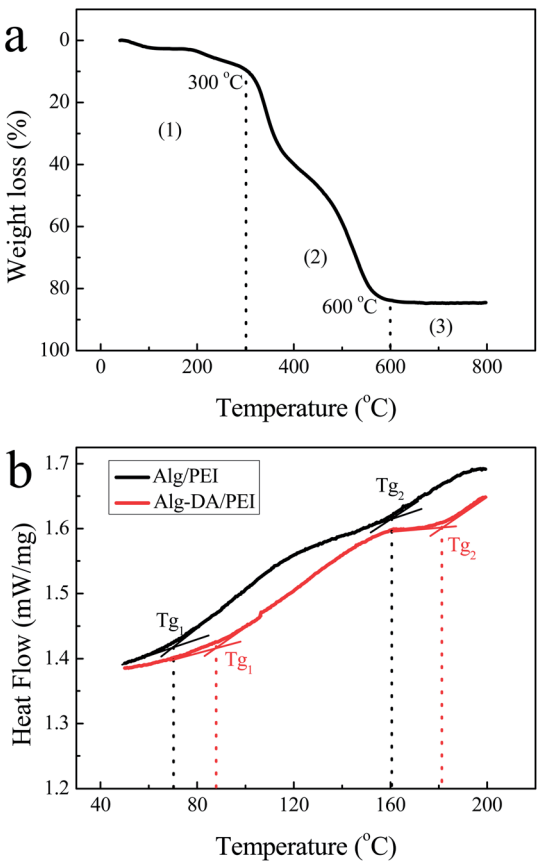

Fig. 7 TGA curve of $(PEI/Alg\text{-}DA)_1PEI$/silica microcapsules (a) and DSC curves of Alg/PEI and Alg-DA/PEI composites (b).

and, another ~75.7% weight loss up to 600 °C (stage 2) was due to the decomposition/degradation of the encapsulated PSS, and the inner (PEI/Alg-DA)/PEI organic layer. The residual ~15.5% weight (stage 3) was attributed to the external inorganic silica layer. The DSC curves of PEI/Alg and PEI/Alg-DA composites are shown in Fig. 7(b). T_{g_1} and T_{g_2} were the glass transition temperatures of alginate and PEI, respectively. The increased T_{g_1} and T_{g_2} for the PEI/Alg-DA composite compared with those for the PEI/Alg composite confirmed the formation of covalent bonds between Alg-DA and PEI.

BET analysis was employed to determine the surface area and pore size distribution of the external silica layer. As shown in Fig. 8, the nitrogen adsorption isotherms of $(PEI/Alg\text{-}DA)_1$/PEI/silica showed the type IV characteristics with a type H3 hysteresis loop, indicating the presence of highly interconnected and slit-shaped pores in the silica shell. The specific surface area and pore size of the silica layer were 26.30 $m^2\ g^{-1}$ and 14.2 nm, respectively. The mesoporous structure of the external inorganic silica layer and the inner organic layer would act as a semipermeable membrane which would allow small molecules (such as substrates and products) to enter and leave the lumen easily while preventing the large encapsulated molecules (such as cell, enzymes) from leaking.

Sufficient mechanical stability of the microcapsules is a prerequisite for practical applications. The mechanical stability of $(PEI/Alg)_2$, $(PEI/Alg\text{-}DA)_2$ and $(PEI/Alg\text{-}DA)_1$/PEI/silica microcapsules was assessed by measuring the penetrated pressure in PSS aqueous solutions with different concentrations. About 200 microcapsules were inspected at each PSS concentration. Microcapsules are generally able to keep their initial shape at low PSS concentrations, but shrunk or broke at high PSS concentrations due to the excess osmotic pressure of the PSS solution under which the large PSS molecules (MW *ca.* 70 000) could not pass through the microcapsule wall. The percentage of deformed microcapsules was usually used as an indicator of the mechanical stability of microcapsules. The percentages of the deformed microcapsules as a function of the PSS concentration are listed in Table 1. In 10% PSS solution, 70% of the total amount of the $(PEI/Alg)_2$ microcapsules were deformed,

Table 1 Percentage of deformed microcapsules as a function of the PSS concentration

PSS concentration (wt%)	$(PEI/Alg)_2$	$(PEI/Alg\text{-}DA)_2$	$(PEI/Alg\text{-}DA)_1$/PEI/silica
10	70% deformed	50% deformed	None
20	100% deformed	100% deformed	None
40	100% deformed	100% deformed	5% deformed

while this deformation percentage decreased to 50% for the $(PEI/Alg\text{-}DA)_2$ microcapsules where dopamine-modified alginate was used instead of alginate. This increase in mechanical strength was due to the stronger interaction between the two self-assembling building blocks, PEI and Alg-DA, as a result of the Michael-type addition and Schiff base reaction occurred between the amine groups of PEI and the catechol groups of Alg-DA. When the concentration of PSS solution was higher than 20%, both the above two kinds of organic microcapsules were deformed totally. The as-prepared organic–inorganic hybrid microcapsules, $(PEI/Alg\text{-}DA)_1$/PEI/silica, showed a fairly good mechanical stability under the same conditions. No deformation was found for the $(PEI/Alg\text{-}DA)_1$/PEI/silica hybrid microcapsules when the PSS concentration was lower than 20%, and only 5% of hybrid microcapsules were deformed when the PSS concentration increased to 40%. The external inorganic silica layer functioned as a dense protective wall and enhanced the mechanical stability of the microcapsules significantly.

A kind of organic–inorganic microcapsules was successfully fabricated through the combination of covalent self-assembly and biomimetic mineralization. The microcapsule had a cell-like structure with a hollow lumen, an organic polymer membrane and an inorganic silica wall. The advantage of the semipermeable organic polymer membrane and the supporting inorganic wall can be utilized to construct a catalysis system. Herein, enzymes were immobilized in the as-fabricated microcapsules and evaluated in the following section.

3.2. Enzyme immobilization application

The hybrid microcapsules were applied for the immobilization of catalase (CAT). CAT was entrapped in the $CaCO_3$ templates during the coprecipitation process and got free in the lumen of the microcapsule after dissolution of the templates. Confocal

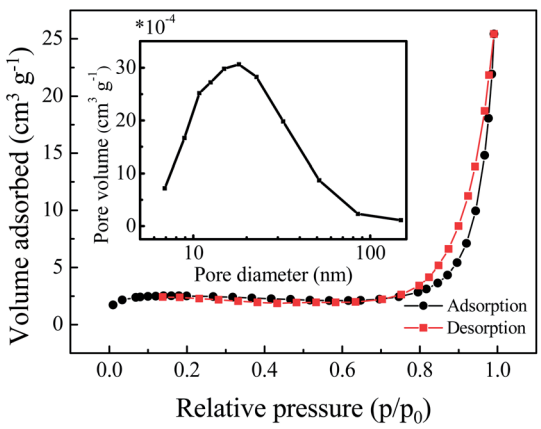

Fig. 8 BJH pore size distribution and N_2 adsorption–desorption isotherm of $(PEI/Alg\text{-}DA)_1$PEI/silica microcapsules.

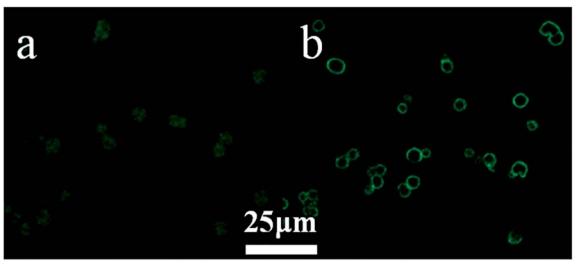

Fig. 9 CLSM images of $CaCO_3$ microspheres (a) and $(PEI/Alg\text{-}DA)_1$PEI/silica microcapsules (b) loaded with FITC-labeled CAT.

Table 2 Activity recovery of CAT in $(PEI/Alg\text{-}DA)_2$ and CAT in $(PEI/Alg\text{-}DA)_1$/PEI/silica

Immobilizate	Immobilization yield	Immobilization efficiency	Activity recovery
CAT-$(PEI/Alg\text{-}DA)_2$	92.6%	14.8%	13.7%
CAT-$(PEI/Alg\text{-}DA)_1$/PEI/silica	93.7%	19.4%	18.2%

Table 3 Kinetic parameters of free CAT, CAT in $(PEI/Alg\text{-}DA)_2$ and CAT in $(PEI/Alg\text{-}DA)_1$/PEI/silica

Enzyme/immobilizate	Free CAT	CAT-$(PEI/Alg\text{-}DA)_2$	CAT-$(PEI/Alg\text{-}DA)_1$/PEI/silica
K_m	50.2	21.8	31.7
V_m	19.4	0.97	2.84

laser scanning microscopy (CLSM) was employed to determine the location of the immobilized enzyme. The fluorescence display of the CAT-containing $CaCO_3$ templates (Fig. 9(a)) revealed the successful immobilization of CAT in the templates. After template removal, the CAT molecules were set free in the lumen and finally enriched around the interior wall of the capsules (Fig. 9(b)) owing to the electrostatic attraction between the positively charged PEI and the negatively charged CAT. In addition, the exposed Alg-DA in the lumen also could grasp CAT through the Michael addition and Schiff base reaction between the amine groups of CAT and the catechol groups of Alg-DA. This was confirmed by the fact that the fluorescence intensity near the wall was slightly higher than that in the interior. The enrichment of CAT to the capsule wall was beneficial for the enzymatic reaction by shortening the diffusion pathway of the substrate and thus making it easier to access the enzyme. For comparison, CAT was also encapsulated in $(PEI/Alg\text{-}DA)_2$ microcapsules according to the same procedure.

The activity recovery values of the immobilized CAT in $(PEI/Alg\text{-}DA)_2$ and $(PEI/Alg\text{-}DA)_1$/PEI/silica microcapsules are shown in Table 2. Immobilization yields of the two microcapsules were both higher than 90%. The immobilization efficiency of CAT in $(PEI/Alg\text{-}DA)_2$ and $(PEI/Alg\text{-}DA)_1$/PEI/silica was 14.8% and 19.4%, respectively. From the perspective of the activity recovery, CAT in $(PEI/Alg\text{-}DA)_1$/PEI/silica was better than that in $(PEI/Alg\text{-}DA)_2$. Kinetic parameters of free CAT, CAT in $(PEI/Alg\text{-}DA)_2$ and $(PEI/Alg\text{-}DA)_1$/PEI/silica are listed in Table 3. K_m values of CAT in the two microcapsules were both lower than the free CAT, suggesting a higher affinity of the enzyme towards the substrate after immobilization. The improved affinity was due to the hydrogen bonds formed between PEI and the substrate H_2O_2 which exerted an enrichment effect of H_2O_2 to the microcapsules, thus increasing the access probability of the substrate molecules to contact CAT near the capsule wall. V_m values of CAT in the two microcapsules were also lower than those of the free CAT, which could be ascribed to the additional diffusion resistance of the capsule wall.

Reusability of immobilized enzymes is a critical aspect in industrial applications. In order to examine the reusability of

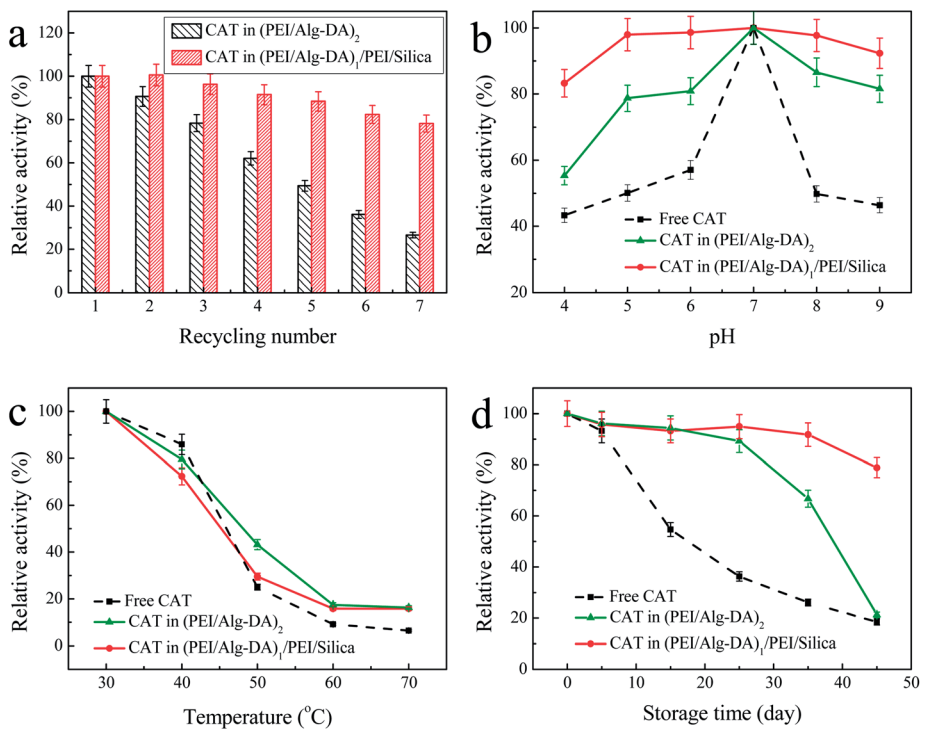

Fig. 10 Recycling stability of encapsulated CAT (a); effect of pH on the activity of free and encapsulated CAT (b); effect of temperature on the activity of free and encapsulated CAT (c); and storage stability of free and encapsulated CAT (d).

the immobilized CAT, the enzyme assay was repeatedly performed by using the same batch of microcapsules. The assay-regeneration cycle was performed 7 times. At the end of each cycle, the immobilized CAT was recovered by centrifugation and washed with 7 mL Tris buffer (0.05 M, pH 7.0) for the next reaction cycle. As illustrated in Fig. 10(a), the CAT immobilized in $(PEI/Alg\text{-}DA)_1/PEI/silica$ showed a much higher reusability than the CAT in $(PEI/Alg\text{-}DA)_2$ due to the enhanced mechanical stability of the hybrid microcapsules which efficiently prevented the rupture of the capsules under reaction conditions with stirring.

The pH stability of CAT in $(PEI/Alg\text{-}DA)_2$ and $(PEI/Alg\text{-}DA)_1/PEI/silica$ microcapsules and the free CAT is compared in Fig. 10(b). After incubation in acetate buffer solution at pH 4.0 for 2 h, the free CAT retained 43% of its initial activity, while the immobilized CAT in $(PEI/Alg\text{-}DA)_2$ and $(PEI/Alg\text{-}DA)_1/PEI/silica$ microcapsules retained more than 55% of its initial activity. After incubation in Tris buffer solution at pH 9.0 for 2 h, the free CAT retained 46% of its initial activity, while the CAT in $(PEI/Alg\text{-}DA)_2$ and $(PEI/Alg\text{-}DA)_1/PEI/silica$ microcapsules retained 81% and 92% of its initial activity, respectively. The reason for the improvement in pH stability of immobilized CAT could be explained by the buffering effect of the organic layer of the microcapsules. The abundant $-COO^-/-COOH$ pairs on Alg-DA and the $-NH_2/-NH_3^+$ pairs on PEI could tune the local pH value in a desirable range. Under basic conditions, the local pH value around the organic layer was lower than the bulk solution, while under acidic conditions, it was higher than the bulk solution. The enrichment of CAT near the polymer capsule membrane kept the enzyme molecules staying within the buffer region, thus minimizing the risk of denaturation. In addition, it has been proved that biosilica itself was also an effective buffer.[38] Therefore, the CAT immobilized in $(PEI/Alg\text{-}DA)_1/PEI/silica$ capsules showed a higher pH stability than the CAT in $(PEI/Alg\text{-}DA)_2$ capsules.

After incubation at high temperatures for 2 h, the immobilized CAT showed a higher residual activity than the free CAT (Fig. 10(c)). The capsule wall seemed to be helpful in maintaining the protein structure from denaturation at high temperatures. The storage stability of CAT encapsulated in $(PEI/Alg\text{-}DA)_2$ and $(PEI/Alg\text{-}DA)_1/PEI/silica$ microcapsules and that of free CAT are compared in Fig. 10(d). The free CAT retained only 27% of its initial activity after storing for 35 days. The CAT immobilized in $(PEI/Alg\text{-}DA)_2$ retained 68% of its initial activity after storing for the same period. In contrast, the storage stability of CAT in $(PEI/Alg\text{-}DA)_1/PEI/silica$ microcapsules was significantly improved with a remarkably lower decreasing rate. The storage efficiency of the enzyme immobilized in the hybrid capsules was as high as 78% of its initial activity after storing for 45 days. All the above enhancements in stability suggested that the hybrid microcapsules could provide a more suitable microenvironment for the enzymes inside. The inner organic layer composed of PEI and dopamine-modified alginate had a high biocompatibility to the immobilized enzyme. The external inorganic silica layer could not only protect the enzyme inside physically, but also prevent them from being attacked by the bacteria in the bulk solution during storage.

4. Conclusions

A mild and efficient method for the construction of robust organic–inorganic hybrid microcapsules was developed by merging of covalent cross-linking and biomimetic mineralization into an LBL self-assembly process. The inner organic layer (PEI/Alg-DA/PEI) was pre-assembled by electrostatic attraction followed by cross-linking through the Michael-type addition and Schiff base reaction between the catechol groups of Alg-DA and the amine groups of PEI. The outmost self-assembly sublayer, PEI, further induced the hydrolysis and condensation of silicic acid to form the outermost inorganic layer (silica). The as-prepared capsules were used to immobilize catalase. The biocompatible inner organic layer created an appropriate microenvironment for the enzyme inside, while the inorganic layer functioned as a protective supporting wall to maintain the intact morphology of the microcapsules. The immobilized CAT in the hybrid capsules exhibited significantly improved pH, thermal, recycling and storage stability. It is reasonable to believe that the dual functions of PEI or other polymers with sufficient amine groups that can not only cross-link with dopamine-modified alginate, but also induce the mineralization of silicate or other inorganic precursors, are useful to further develop the self-assembly technique for the construction of robust hybrid microcapsules.

Conflict of interest

The authors declare no competing financial interest.

Acknowledgements

The authors thank the financial support from the Program for New Century Excellent Talents in University (NCET-10-0623), the Specialized Research Fund for the Doctoral Program of Higher Education, the National Science Foundation of China (21076145), the National Science Fund for Distinguished Young Scholars (21125627) and the Program of Introducing Talents of Discipline to Universities (B06006).

References

1 W. J. Tong, X. X. Song and C. Y. Gao, *Chem. Soc. Rev.*, 2012, **41**, 6103–6124.
2 R. C. Luo, S. S. Venkatraman and B. Neu, *Biomacromolecules*, 2013, **14**, 2262–2271.
3 G. Decher and J. D. Hong, *Makromol. Chem., Macromol. Symp.*, 1991, **46**, 321–327.
4 O. S. Sakr and G. Borchard, *Biomacromolecules*, 2013, **14**, 2117–2135.
5 Y. J. Wang, A. S. Angelatos and F. Caruso, *Chem. Mater.*, 2008, **20**, 848–858.
6 G. Decher, *Science*, 1997, **277**, 1232–1237.
7 Y. P. Tan, U. H. Yildiz, W. Wei, J. H. Waite and A. Miserez, *Biomacromolecules*, 2013, **14**, 1715–1726.
8 B.-S. Kim, S. W. Park and P. T. Hammond, *ACS Nano*, 2008, **2**, 386–392.

9 J. L. Lutkenhaus, K. D. Hrabak, K. McEnnis and P. T. Hammond, *J. Am. Chem. Soc.*, 2005, **127**, 17228–17234.
10 H. Ejima, J. J. Richardson, K. Liang, J. P. Best, M. P. van Koeverden, G. K. Such, J. W. Cui and F. Caruso, *Science*, 2013, **341**, 154–157.
11 X. L. Wang, Z. Y. Jiang, J. F. Shi, Y. P. Liang, C. H. Zhang and H. Wu, *ACS Appl. Mater. Interfaces*, 2012, **4**, 3476–3483.
12 M. Tagliazucchi, V. A. Amin, S. T. Schneebeli, J. F. Stoddart and E. A. Weiss, *Adv. Mater.*, 2012, **24**, 3617–3621.
13 B. Samanta, X.-C. Yang, Y. Ofir, M.-H. Park, D. Patra, S. S. Agasti, O. R. Miranda, Z.-H. Mo and V. M. Rotello, *Angew. Chem., Int. Ed.*, 2009, **48**, 5341–5344.
14 X. L. Feng, A. Curnurcu, X. F. Sui, J. Song, M. A. Hernpenius and G. J. Vancso, *Langmuir*, 2013, **29**, 7257–7265.
15 S. L. Bechler and D. M. Lynn, *Biomacromolecules*, 2012, **13**, 1523–1532.
16 X. Y. Zhu, S. F. Guo, D. Janczewski, F. J. P. Velandia, S. L.-M. Teo and G. J. Vancso, *ACS Appl. Mater. Interfaces*, 2013, **5**, 5961–5968.
17 Q. Y. Yi, D. S. Wen and G. B. Sukhorukov, *Langmuir*, 2012, **28**, 10822–10829.
18 H. Lee, J. Rho and P. B. Messersmith, *Adv. Mater.*, 2009, **21**, 431–434.
19 H. Lee, S. M. Dellatore, W. M. Miller and P. B. Messersmith, *Science*, 2007, **318**, 426–430.
20 H. Lee, B. P. Lee and P. B. Messersmith, *Nature*, 2007, **448**, 338–341.
21 J. W. Cui, Y. Yan, G. K. Such, K. Liang, C. J. Ochs, A. Postma and F. Caruso, *Biomacromolecules*, 2012, **13**, 2225–2228.
22 L. Zhang, J. F. Shi, Z. Y. Jiang, Y. J. Jiang, S. Z. Qiao, J. Li, R. Wang, R. Meng, Y. Y. Zhu and Y. Zheng, *Green Chem.*, 2011, **13**, 300–306.
23 J. W. Cui, Y. J. Wang, A. Postma, J. C. Hao, L. Hosta-Rigau and F. Caruso, *Adv. Funct. Mater.*, 2010, **20**, 1625–1631.
24 C. Lee, J. Shin, J. S. Lee, E. Byun, J. H. Ryu, S. H. Um, D.-I. Kim, H. Lee and S.-W. Cho, *Biomacromolecules*, 2013, **14**, 2004–2013.
25 Q. S. Wen, L. B. Liu, Q. Yang, F. T. Lv and S. Wang, *Adv. Funct. Mater.*, 2013, **23**, 764–769.
26 S. J. Clarke, C. A. Hollmann, Z. J. Zhang, D. Suffern, S. E. Bradforth, N. M. Dimitrijevic, W. G. Minarik and J. L. Nadeau, *Nat. Mater.*, 2006, **5**, 409–417.
27 R. Qiao, X. L. Zhang, R. Qiu, J. C. Kim and Y. S. Kang, *Chem. Mater.*, 2007, **19**, 6485–6491.
28 W. Yuan, Z. Lu and C. M. Li, *J. Mater. Chem.*, 2011, **21**, 5148–5155.
29 J. Li, Z. Y. Jiang, H. Wu, L. Zhang, L. H. Long and Y. J. Jiang, *Soft Matter*, 2010, **6**, 542–550.
30 M. Sumper and E. Brunner, *Adv. Funct. Mater.*, 2006, **16**, 17–26.
31 N. Kroger, R. Deutzmann and M. Sumper, *Science*, 1999, **286**, 1129–1132.
32 K. E. Cole, A. N. Ortiz, M. A. Schoonen and A. M. Valentine, *Chem. Mater.*, 2006, **18**, 4592–4599.
33 S. V. Patwardhan and S. J. Clarson, *J. Inorg. Organomet. Polym.*, 2003, **13**, 193–203.
34 S. V. Patwardhan, R. Maheshwari, N. Mukherjee, K. L. Kiick and S. J. Clarson, *Biomacromolecules*, 2006, **7**, 491–497.
35 J.-S. Jan, P.-S. Chen, P.-L. Hsieh and B.-Y. Chen, *ACS Appl. Mater. Interfaces*, 2012, **4**, 6864–6873.
36 Y. J. Jiang, D. Yang, L. Zhang, Q. Y. Sun, X. H. Sun, J. Li and Z. Y. Jiang, *Adv. Funct. Mater.*, 2009, **19**, 150–156.
37 J.-W. Shen, C. L. Li, N. F. A. V. D. Vegt and C. Peter, *J. Phys. Chem. C*, 2013, **117**, 6904–6913.
38 A. J. Milligan and F. M. M. Morel, *Science*, 2002, **297**, 1848–1850.